Journal of Applied Physics ARTICLE pubs.aip.org/aip/jap

Atomic layer deposition of HfO_2 as a charge-lean capping layer material for SiO_2-modulation acceptor doping of silicon

Cite as: J. Appl. Phys. **137**, 064301 (2025); doi: 10.1063/5.0256687
Submitted: 6 January 2025 · Accepted: 13 January 2025 ·
Published Online: 10 February 2025

View Online Export Citation CrossMark

Somayeh Shams, Ingmar Ratschinski, and Daniel Hiller[a)]

AFFILIATIONS

Institute of Applied Physics, Technical University Bergakademie Freiberg, Freiberg, Germany

[a)]**Author to whom correspondence should be addressed:** Daniel.Hiller@physik.tu-freiberg.de

ABSTRACT

Modulation doping of SiO_2 by Al-induced acceptor states is a promising alternative to conventional impurity doping for silicon nanostructures, enabling the introduction of free holes in Si without direct impurity incorporation into the lattice. SiO_2 modulation doping of Si is achieved by a short high-temperature anneal of a tunnel-SiO_2 layer coated with an AlO_x monolayer by atomic layer deposition (ALD). However, this ultra-thin modulation doping (MD) stack is highly susceptible to degradation when exposed to ambient air. In this work, we investigated ALD hafnium oxide (HfO_2) as a reliable, charge-lean capping layer to protect the MD stack and preserve its doping properties. We optimized the ALD-HfO_2 deposition process using tetrakis(ethylmethylamino)hafnium (TEMAHf) and various oxygen co-reactants (H_2O, O_3, O_2-plasma) as well as different deposition temperatures and studied the effects of post-deposition RTA. Thermal ALD with H_2O as the oxygen reactant at 200 °C yields HfO_2 films with superior electrical properties, including low positive fixed charge densities ($<1 \times 10^{12}$ cm^{-2}), minimal hysteresis, and high permittivity ($\varepsilon = 17$). The optimized HfO_2 film was successfully integrated into modulation-doped metal–oxide–semiconductor capacitors (MD MOS-caps) to evaluate their effectiveness as capping layers. Notably, *in situ* capping, where the HfO_2 layer is deposited immediately after the AlO_X without breaking vacuum, results in higher modulation doping efficiency and demonstrated higher negative fixed charge densities compared to *ex situ* capping. These findings demonstrate that optimized ALD-HfO_2 can serve as a charge-lean capping material, enhancing the stability and performance of modulation-doped Si nanostructures by effectively protecting the ultra-thin MD stack from ambient degradation.

I. INTRODUCTION

Silicon nanowires (Si NWs) and nanosheets are integral building blocks for future transistors and nanoelectronic devices due to their great potential for further scaling.[1,2] However, conventional impurity doping methods such as implantation, monolayer doping, and gas-phase doping become increasingly inefficient for these ultra-small nanostructures. Gas-phase doping[3] requires a high thermal budget, resulting in large dopant diffusion lengths that are incompatible with nano-junction scaling. Likewise, monolayer doping (MLD)[4,5] relies on a rapid thermal anneal (RTA) to drive dopants from the monolayer into Si, which can lead to excessive diffusion. These methods depend on incorporating impurity dopants into the silicon lattice and, therefore, do not fully address the challenges of nano-scale doping. In nanostructures, these processes are impeded by quantum confinement effects and interactions with interface defects.[6–10] Furthermore, ultra-small semiconductor volumes are affected by dopant fingerprint effects caused by Poisson statistics of the distribution of the few dopants involved.[11,12] Although purely electrostatic[13] or charge-transfer doping[14,15] can sidestep some thermal issues, they often demand constant external fields or tightly controlled surface chemistries–factors that limit their stability and integration prospects. Consequently, alternative doping methods are needed that can effectively introduce free carriers without relying on impurity incorporation into the silicon lattice.

Modulation doping is a promising alternative, offering a means to spatially separate the free carriers from their parent dopant atoms. In previous work,[10] we proposed the modulation

acceptor doping of silicon by utilizing aluminum-induced acceptor states in an adjacent SiO_2 layer. The basic modulation doping (MD) stack consists of a ~2 nm thick tunnel SiO_2 layer coated with a few cycles of atomic layer deposition (ALD) of AlO_X. A short thermal treatment induces acceptor states in the SiO_2 with an energy level of ~0.5 eV below the Si valence band edge. Electrons relaxing from the Si valence band into these acceptor states provide holes to the Si that do not require constant thermal ionization, which implicates the absence of doping freeze-out effects at cryogenic temperatures. On the other hand, the ionized acceptor states in SiO_2 (forming a negative fixed charge Q_{fix} in the oxide) cause an electric field that energetically lifts the yet unoccupied acceptor states in the vicinity and prevents their ionization via a Coulomb repulsion effect. Since the fraction of ionized Al-induced acceptor states is rather small,[10,16] the modulation acceptor doping process provides a self-regulating hole density based on the surface-to-volume ratio—and not dependent on the exact number of dopant atoms.

Recently, we have demonstrated that modulation-doped Si NWs with Al-doped SiO_2 shells (SiO_2:Al) exhibit electrical resistances several orders of magnitude lower than Si NWs with undoped SiO_2 shells.[17,18] Specifically, these modulation-doped Si NWs achieved surface-induced free carrier densities reaching approximately 10^{18} cm^{-3}, which significantly enhances their conductivity. Despite these advancements, a critical challenge remains: the conductivity of modulation-doped Si NWs deteriorates over several days of storage. This degradation is attributed to interactions with ambient air, which can lead to the formation of unwanted surface states and the deterioration of the ultra-thin SiO_2:Al stack. Therefore, a suitable capping layer is essential to protect the modulation-doped structures from environmental factors. The capping material must be lean of fixed charges to avoid interference with the modulation doping mechanism or Q_{fix}-induced shifts of device thresholds.[19] ALD hafnium oxide (ALD-HfO_2) would be a promising candidate for the capping material due to its excellent dielectric properties, thermal stability, and compatibility with Si-based technologies.[20–23] The introduction of a dielectric capping layer not only serves as a protective barrier but also enables the formation of metal–oxide–semiconductor (MOS) capacitor stacks with sufficient thickness for, e.g., capacitance–voltage (C–V) measurements. This allows for a comprehensive characterization of the electrical properties of the ALD-HfO_2 as a capping material that enhances the stability, reliability, and charge-lean characteristics of modulation-doped Si nanostructures. However, initially optimizing this material to achieve the lowest possible fixed charge density and sufficient electrical breakdown resistance is crucial for preserving the enhanced electrical properties of modulation-doped Si nanostructures. In this work, first we focus on the optimization of ALD-HfO_2 by the investigation of the deposition conditions, such as choice of oxygen co-reactant, deposition temperature, and post-annealing treatment. Then, we examine the performance of the optimized ALD-HfO_2 as the capping layer for the underlying SiO_2:Al stack in MD MOS-caps. We also report a first examination of this capping layer and its role in the modulation doping mechanism via the comparison of *ex situ* capping and *in situ* capping deposition.

II. EXPERIMENTAL DETAILS

Initially, atomic layer deposition HfO_2 thin films on silicon substrates was optimized using a Beneq-R2 system and the oxygen reactants, water (H_2O) and ozone (O_3) for thermal ALD (TALD), and oxygen (O_2) plasma for plasma-enhanced ALD (PEALD). Subsequently, the HfO_2 films were deposited on bulk-Si wafers and MOS-caps of type-A configuration (Fig. 1) were characterized by C–V, I–V, and x-ray measurements. Finally, the best HfO_2 capping was applied to the modulation-doped (MD) MOS-caps of type-B (Fig. 1).

The substrates used in this study were single-side polished, ⟨100⟩-oriented CZ-Si wafers with *n*-type doping (phosphorus) of 1–20 Ω cm resistivity and *p*-type doping (Boron) of >1 Ω cm resistivity. The wafers were cleaned using the standard Radio Corporation of America (RCA) process. For some wafers, the thin hydrophilic oxide grown in the RCA-2 solution was preserved, whereas others received a final dip in diluted HF to prepare a hydrophobic H-terminated Si surface (labeled HF-last). The hafnium precursor used was tetrakis(ethylmethylamino)hafnium (TEMAHf) heated to 90 °C in a vapor draw container. Nitrogen gas for the thermal ALD processes and argon for the plasma-based depositions were used as purge and carrier gases, respectively. Each deposition cycle consisted of a hafnium precursor pulse (2 s), purging (3 s), oxygen co-reactant pulse (100 ms for H_2O/3 s for O_3/3 s for O_2-plasma), and oxidant purging (5 s for H_2O/7 s for O_3/10 s for O_2-plasma). The capacitively coupled RF plasma power for PEALD was 50 W. Note that the maximum deposition temperature in the plasma configuration of the chamber is limited to 250 °C.

Some of the HfO_2 films dedicated to C–V measurements in MOS-cap type-A configuration were subjected to post-deposition annealing identical to the one routinely used for activating and ionizing the Al-induced acceptor states in SiO_2. Thereby, the influence of this anneal on the dedicated capping material was studied.

For the MD MOS-caps of type-B, HF-last Si substrates were rapidly thermally oxidized (RTO) to obtain a 2.2 nm thick tunnel-SiO_2 layer. Trimethylaluminum (TMA) and H_2O AlO_x monolayers of 5, 7, and 10 ALD-cycles were deposited at 200 °C. For reference samples without modulation doping, the tunnel-oxide coated wafers were only subjected to H_2O pulses in the ALD chamber without growing any AlO_x. Eventually, 15 nm of the optimized HfO_2 capping layer was deposited in the same ALD

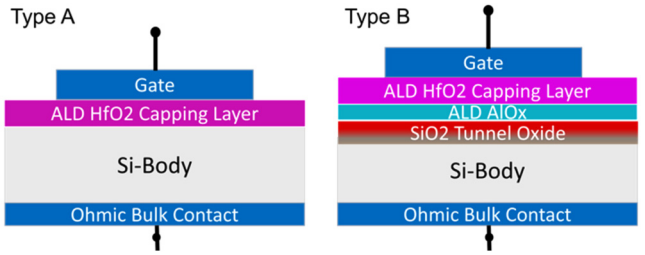

FIG. 1. MOS-cap type-A, ALD-HfO_2 on bare Si body, and MOS-cap type-B, ALD-HfO_2 on MD stack comprising of SiO_2 tunnel oxide and ALD-AlO_X monolayers.

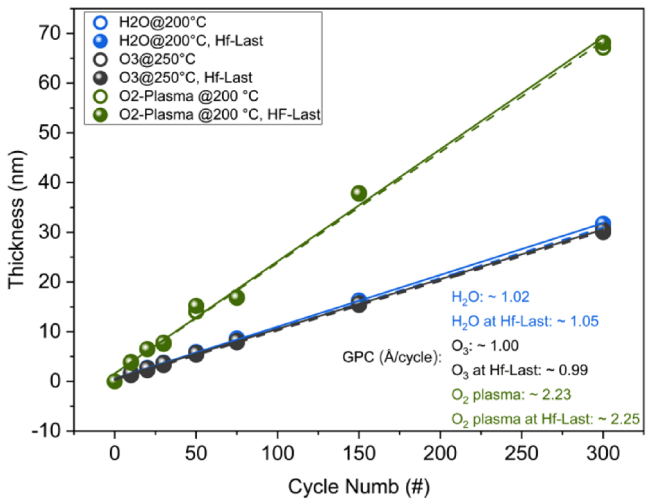

FIG. 2. Thickness of deposited ALD-HfO_2 as function of cycle number and different oxygen co-reactants, H_2O, O_3, and O_2-plasma on both hydrophilic RCA-2-last (empty circles indicate the experimental data points and dashed lines indicate the attributed linear fitting) and HF-last (solid circles and solid fitted lines) Si surfaces.

chamber. In case the samples were exposed to ambient air between the depositions of the AlO_x monolayers and the HfO_2 capping, we refer to these as "*ex situ*." Samples with an immediate HfO_2 capping deposition without breaking the vacuum are labeled "*in situ*." The final MD-activation was accomplished by rapid thermal annealing (RTA) at 850 °C for 30 s in an Ar atmosphere. The aluminum contacts on the front side of the samples were thermally evaporated through a shadow mask, whereas the substrate backside was full-area metallized.

All HfO_2 thicknesses were measured by variable angle spectroscopic ellipsometry (VASE, Woollam M-2000; spectral range 250–1000 nm, angles: 70°, 75°, 80°) using a Tauc–Lorentz model. X-ray reflectivity (XRR) and x-ray diffraction (XRD) measurements were performed using a Bruker D8 Advance diffractometer (Cu K-alpha line). High frequency (100 kHz) capacitance–voltage (C–V) measurements were carried out using a Agilent E4980A Precision LCR Meter to evaluate the fixed charge density (Q_{fix}), permittivity, and hysteresis between forward and reverse bias sweeps. Current–voltage (I–V) measurements were performed using the same device to determine the breakdown field and study the breakdown and charge trapping behavior.

III. RESULTS AND DISCUSSION

A. ALD-HfO_2 process development

We investigated the atomic layer deposition of HfO_2 using tetrakis(ethylmethylamino)hafnium (TEMAHf) as the hafnium precursor[24] and optimized the deposition parameters. The key findings of the optimization are presented here, while additional details on the optimization and supporting data can be found in the supplementary material. In Fig. 2, the linearity of the growth-per-cycle (GPC) vs the number of ALD-cycles for these three processes is shown on both hydrophilic RCA-2 last Si and hydrophobic HF-last Si. The GPC for both TALD films with H_2O and O_3 co-reactants deposited at 200 and 250 °C, respectively, is ca. 1 Å/cycle. In contrast, the GPC for the PEALD processes at 200 °C around 2 Å/cycle. The higher GPC for PEALD is consistent with previous reports in the literature.[25,26] Obviously, TEMAHf has no significant growth delay on the H-terminated Si surface and within error bars, the GPCs on both Si surfaces are the same.

B. Properties of ALD-HfO_2 on bare Si (MOS-cap type-A)

In Fig. 3, representative C–V curves of approximately 20 nm ALD-HfO_2 films deposited on HF-last Si in MOS-cap type-A configuration are shown. The panels show HfO_2 grown by all three oxidants at different deposition temperatures for as-deposited (AD) and after the post-anneal (RTA). As can be seen from the C–V curve shape, the lower temperature O_3-processes cause kinks near accumulation indicating defect states. For the PEALD processes, the transition of the C–V curves from inversion to accumulation is

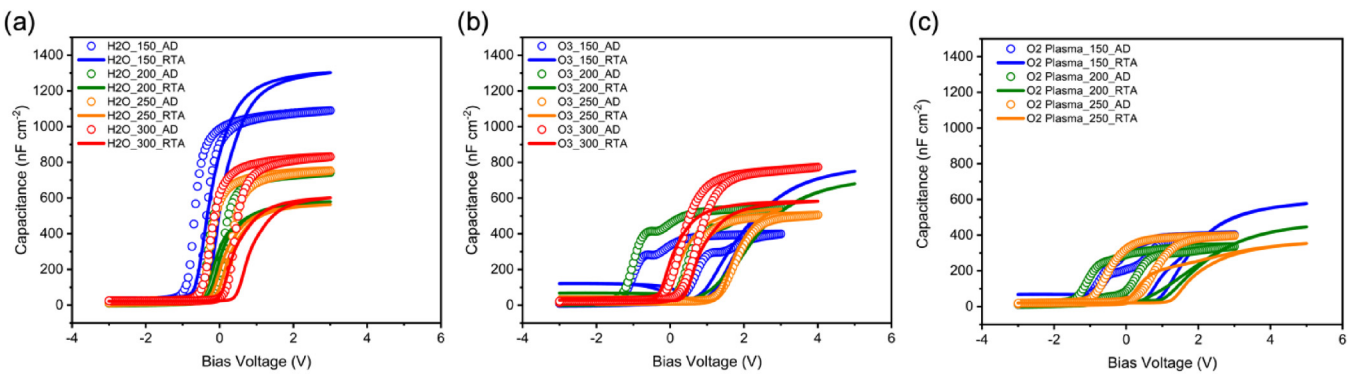

FIG. 3. High frequency C–V curves of ALD-HfO_2 films deposited on Si in MOS-cap type-A configuration for as-deposited (AD) and post-annealed (RTA) HfO_2 films using H_2O (a), O_3 (b), and O_2-plasma (c) co-reactants as a function of deposition temperature.

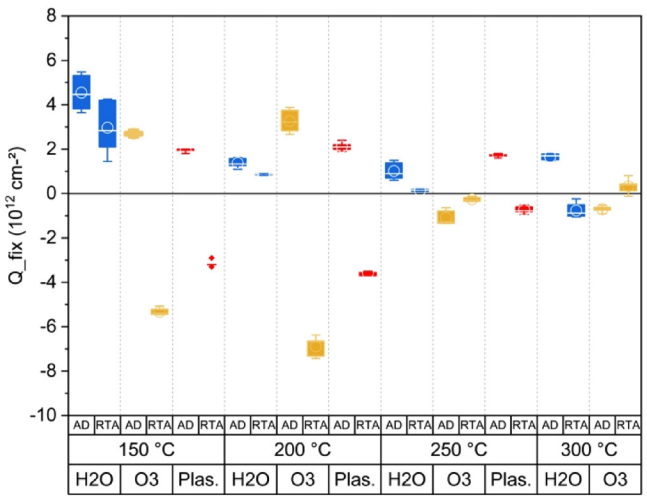

FIG. 4. Oxide fixed charge density (Q_{fix}) extracted from the C–V measurement of ALD-HfO_2 films deposited in MOS-cap type-A configuration for as-deposited (AD) and post-annealed (RTA) HfO_2 films using H_2O, O_3, and O_2-plasma co-reactants as a function of deposition temperature.

not steep, which points toward high densities of interface traps. For all H_2O-grown films, however, steep C–V curves without kinks are observed.

H_2O-based oxide films also show remarkably smaller hysteresis (ca. 100 mV for annealed samples) at deposition temperatures of 200 and 250 °C, indicating a more stable interface with reduced charge trapping. Another key quality criterion concerns the flat-band voltage of the C–V curves and the related oxide fixed charge density. Figure 4 shows Q_{fix} extracted from on average five C–V measurements on each sample. O_3 has a fluctuating Q_{fix} polarity, and a low density of Q_{fix} is only achieved for rather high deposition temperatures. O_2-plasma results in positive Q_{fix} for as-deposited HfO_2 and transitions to negative Q_{fix} after RTA. This indicates an instability in the charge characteristics that could compromise device reliability. In contrast, H_2O at 200 or 250 °C consistently provided small positive Q_{fix} densities below $+1 \times 10^{12}\,cm^{-2}$, both before and after RTA. The TALD H_2O-based HfO_2 films at medium deposition temperatures appear to be the most electrically promising candidates for the use as a charge-lean capping material.

In addition, these films achieved the highest values of permittivity (up to $\varepsilon = 17$, Fig. S1 in the supplementary material), along with a refractive index (n) of around 2.14 at a wavelength of 632.8 nm (according to ellipsometry, Fig. S2 in the supplementary material).

The long-term reliability of these samples was evaluated through electrical characterization after a one-year period of storage under ambient conditions by hf C–V measurements over five contacts for each sample. The C–V curves [Figs. 5(a) and 5(b)] show slight changes in the accumulation capacitance (C_{OX}) in both directions, in the range of around −3% to +12% across different samples. Despite these small numerical variations in C_{OX} values, the hysteresis characteristics remained unchanged throughout the aging period for all samples, indicating consistent charge trapping behavior. In Fig. 5(c), the Q_{fix} distribution shows negligible variation between new and aged samples. The bidirectional nature of the C_{OX} changes, combined with the consistency in both hysteresis and fixed charge characteristics, strongly suggests that the observed variations fall within experimental uncertainty ranges rather than indicating any systematic degradation. These results demonstrate that the performance of the devices capped by the TALD H_2O-based HfO_2 films at 200 and 250 °C deposition temperatures remained reliable over the one-year period under ambient conditions.

In order to study the morphology of the H_2O-HfO_2 thin films and especially the impact of the 850 °C RTA, XRD was measured for ca. 5, 15, and 30 nm thick films grown by the H_2O process at 200 °C. As determined by XRD characterization (Fig. 6), all as-deposited films are amorphous, while the annealed counterparts

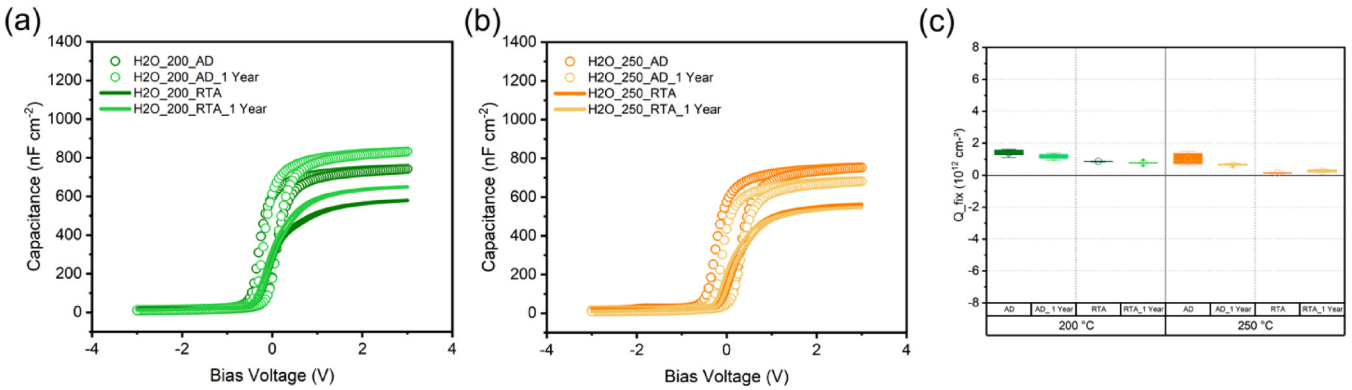

FIG. 5. High frequency C–V measurement as a long-term reliability test of TALD H_2O-based HfO_2 films deposited on Si in MOS-cap type-A configuration, for as-deposited and post-annealed samples. Comparison between fresh and one-year aged samples: (a) C–V curves of films deposited at 200 °C, (b) C–V curves of samples deposited at 250 °C, (c) Q_{fix} distributions extracted from C–V measurements.

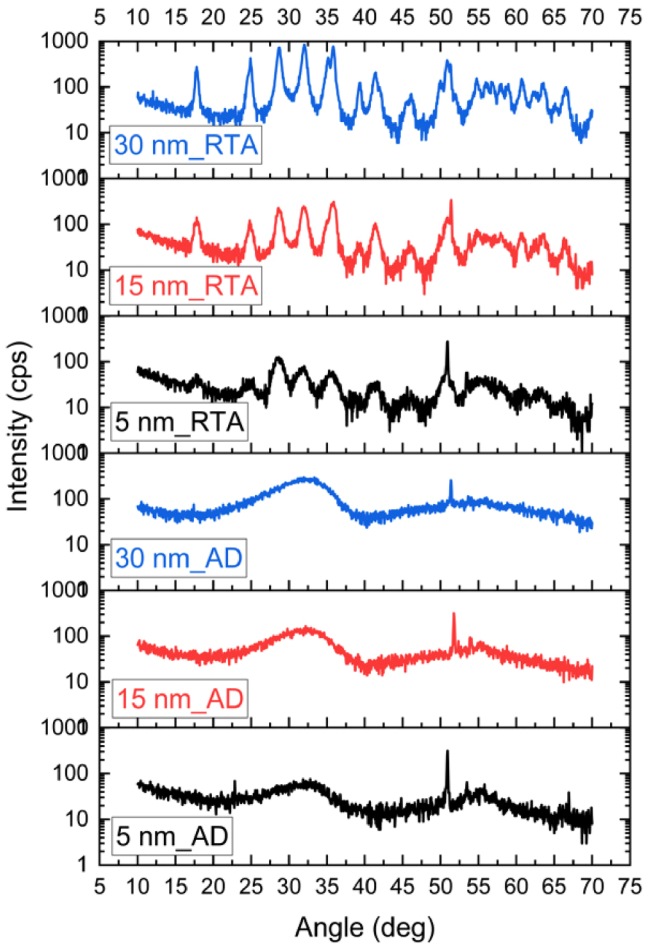

FIG. 6. X-ray diffraction patterns of TALD-HfO_2 films deposited at 200 °C using H_2O as a co-reactant, shown for thicknesses of approximately 5, 15, and 30 nm under as-deposited (AD) and post-annealed (RTA) conditions. As-deposited films are amorphous, while post-annealed samples exhibit the monoclinic HfO_2 phase.

are crystallized even the thinnest (5 nm) film. The peak intensity dramatically increases with film thickness and more peaks become distinguishable, indicating increased crystallite size. Fitting with ICSD 60902 (card reference from ICSD database), all the peaks can be indexed to the monoclinic HfO_2 (P121/c1),[27] ruling out any secondary phases. The feature located at angle 51° can be attributed to the (311) plane of the underlying Si (100) substrate. According to the Scherrer analysis of the peak widths, the obtained crystallite sizes in the annealed films are 4.7, 7.5, and 11.2 nm for the layer thicknesses of ca. 5, 15, and 30 nm, respectively. According to XRR (please see Fig. S3 in the supplementary material), the annealing decreases the thickness only insignificantly in the range of 2%–7%, whereas the density increases to around 9.5 g/cm^3, close to the theoretical density of bulk HfO_2, which is around 9.68 g/cm^3 and higher than previous reports.[26,28,29] The fitted XRR surface roughness decreases after annealing and increases with thickness, as indicated by the root mean square (rms) roughness value of 0.4, 0.8, and 1.7 nm for the annealed films with thickness 5, 15, and 30 nm, respectively.

The C–V curves of these layers are presented in Fig. 7(a) and the extracted Q_{fix} (attributed to the shift of flatband voltage V_{FB} in the forward sweep) in Fig. 7(b). The HfO_2 thickness variation reveals that the C–V hysteresis increases with thickness, even though the same electric fields were applied at the maximum bias in accumulation. The hysteresis is always clockwise, indicating the trapping of electrons from the *n*-type substrate in the HfO_2 thin films. The increasing magnitude of the hysteresis with increasing film thickness indicates a higher density of trapping states in thicker oxide films. Extracting the averages trapped charge (electron) densities yields values of around 1×10^{12} cm^{-2} for the both as-deposited and annealed 5 nm and increase to around 5×10^{12} cm^{-2} and 8.5×10^{12} cm^{-2} for the as-deposited and annealed samples with a thickness of 30 nm, respectively. In contrast, Q_{fix} decreases by increasing the thickness from $+4 \times 10^{12}$ cm^{-2} (for 5 nm) to around $+1 \times 10^{12}$ cm^{-2} (30 nm) for as-deposited samples. One reason for this could be that the fixed charges are mainly localized at the HfO_2/Al-contact interface and originate, e.g., from oxygen scavenging Al gate metal.[30] Annealing effectively decreases Q_{fix} with the values of $+2.5 \times 10^{12}$ to $+0.5 \times 10^{12}$ cm^{-2} for 5 and 30 nm dielectric films, respectively.

The electrical breakdown behavior in current–voltage (I–V) measurements on these samples was studied using MOS-cap type-A samples on both n^+ and p^+ doped Si wafers (both with 1–5 mΩ cm resistivity). The single forward sweeps of current density (J) vs electric field (E) into accumulation for both substrate polarities are presented in Fig. 7(c). Surprisingly, the hole leakage currents are higher for thicker HfO_2 films, for both as-deposited and annealed samples. Thicker films, supported by the observed increase in trapping (C–V hysteresis), contain a higher density of bulk defects and trap states, which may facilitate trap-assisted tunneling and contribute to elevated leakage currents despite the increased physical thickness. Moreover, microstructural changes, such as crystallite size and grain boundaries, can introduce additional conduction pathways, especially after annealing. For the electron leakage currents, the same is observed for as-deposited samples, whereas the annealed films show less clearly expressed differences. In addition, the electrical breakdown occurs for all samples at significantly higher electric fields for the 5 nm samples. As shown in Fig. 7(d), breakdown fields increase from ca. 4.5 and 3.5 MV/cm for the as-deposited (30 nm) p^+ and n^+ samples to the values of ca. 7.5 and 5 MV/cm for the as-deposited (5 nm) p^+ and n^+ samples, respectively. As shown (Fig. S4 in the supplementary material), J–E dual sweep trapping measurements show the same trend as the C–V hysteresis, i.e., increasing trapping density with increasing the thickness.

Overall, these results demonstrate that the 200 °C H_2O-ALD-HfO_2 films show reasonable electrical properties for the application as capping layers in MD MOS-caps. However, since in that case, the HfO_2 is not deposited directly on Si but on the tunnel-SiO_2/AlO_X-monolayer stack (MOS-cap type-B), the exact electrical behavior has to be studied.

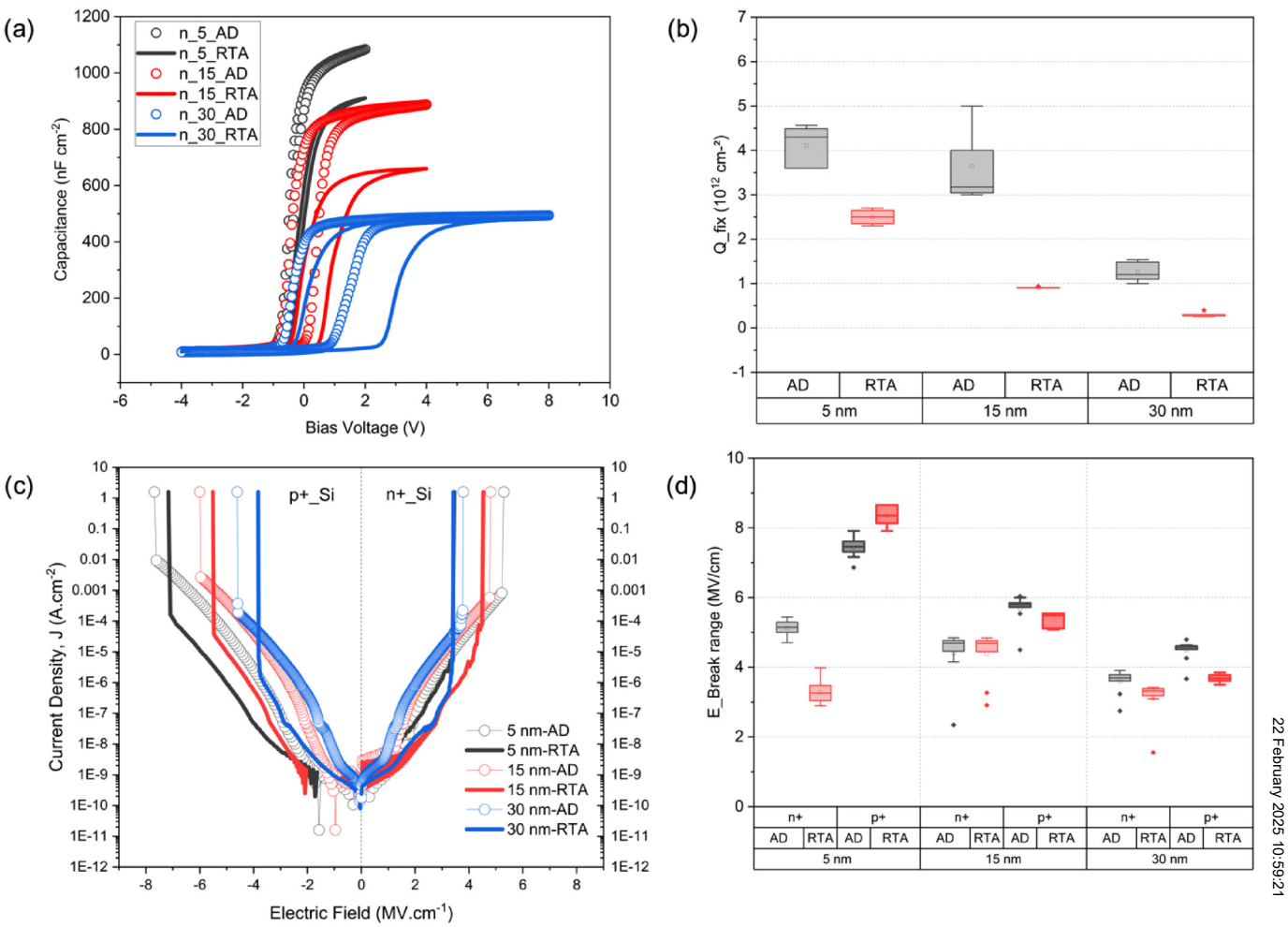

FIG. 7. Electrical characterization of TALD-HfO_2 films deposited with H_2O co-reactant at 200 °C as a function of thickness and annealing in MOS-cap type-A, (a) C–V curves, (b) attributed extracted oxide fixed charge density (Q_{fix}), (c) current density vs electric field, and (d) electric fields breakdown.

C. Properties of ALD-HfO_2 as capping layer (MOS-cap type-B)

The optimized HfO_2 with ca. 15 nm thickness was examined as the capping layer material in MOS-cap type-B samples. Figure 8(a) shows the C–V curves of the reference sample (without ALD-AlO_X layer) and MD-samples (with 2.2 nm tunnel oxide and 5, 7, or 10 cycles of ALD-AlO_X) capped by an *ex situ* ALD-HfO_2 layer (i.e., with breaking the vacuum between AlO_x and HfO_2 deposition). Evident from the C–V curves, the reference samples display a relatively flat inversion region, consistent with our earlier findings. However, in the MD-samples, a slightly elevated inversion capacitance emerges, which we attribute to inversion charges (holes) introduced by the MD stack. These charges can quickly follow the high AC frequencies, which induces a low-frequency-like C–V behavior.

The extracted Q_{fix} of these samples is presented on the left-hand side of Fig. 8(b). The reference sample shows an acceptable positive Q_{fix} density around $+1 \times 10^{12}\,cm^{-2}$, which here also includes fixed charges in the thermal SiO_2. The MD-samples show the typical trend of negative Q_{fix} as a function of ALD-AlO_x cycles with a saturation for seven cycles[16] here at around $-2.5 \times 10^{12}\,cm^{-2}$. Accordingly, the relative Q_{fix} induced by the Al-acceptor states is around $-3.5 \times 10^{12}\,cm^{-2}$. For comparison, in previous studies with PECVD-SiO_2 capping layers, Q_{fix} up to $-5 \times 10^{12}\,cm^{-2}$ was achieved.[10]

However, when considering the Q_{fix} values of the *in situ* process, i.e., without breaking the vacuum between AlO_x and HfO_2 deposition, an 80% higher negative fixed charge is measured, as shown on the right-hand side of Fig. 8(b). However, the *in situ* reference sample has an almost identical positive Q_{fix} as the *ex situ* reference, the 7-cycle *in situ* MD-sample exhibits around

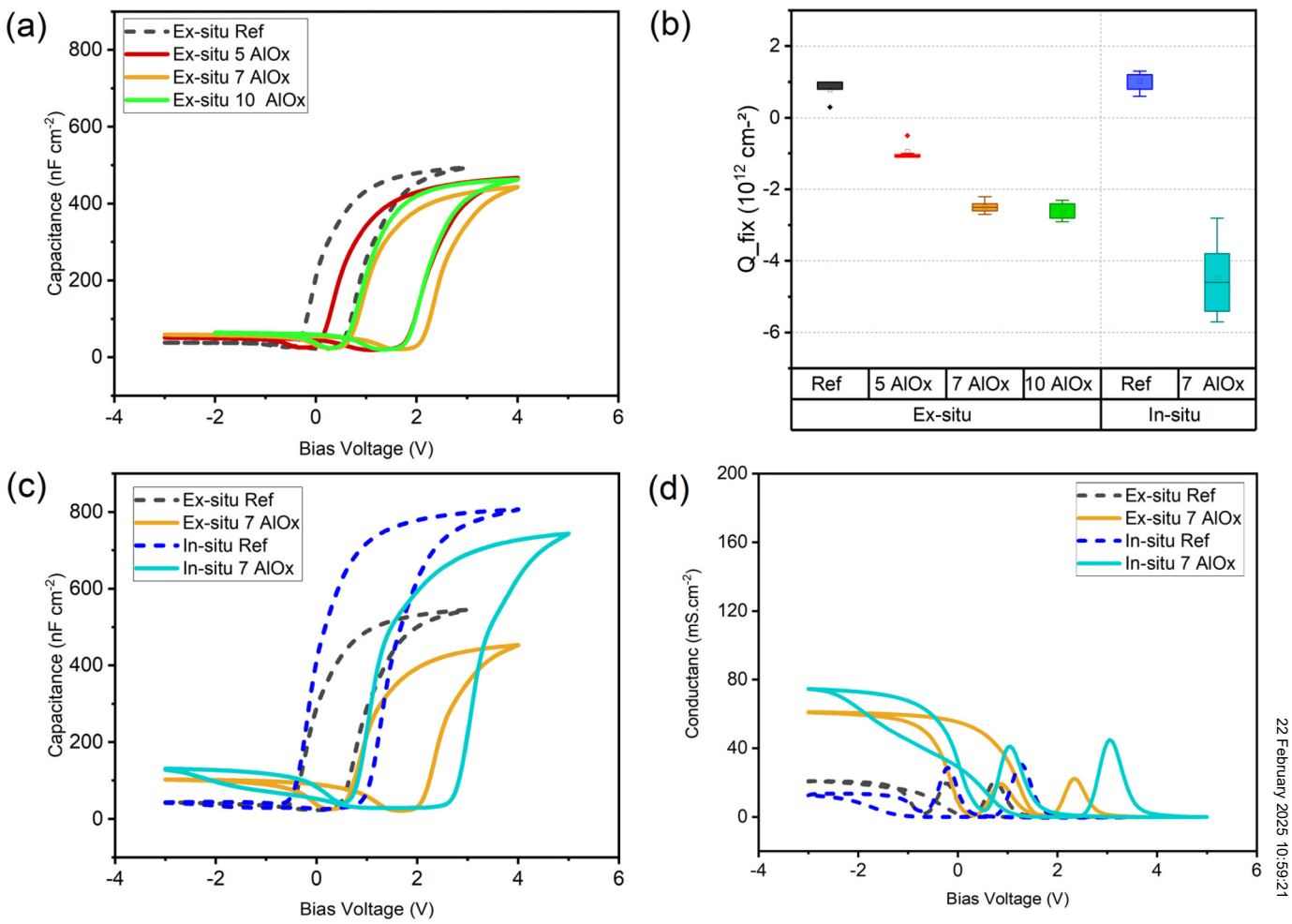

FIG. 8. High frequency C–V measurement of MOS-caps type-B, capped with optimized TALD H_2O-based HfO_2 as the dielectric material. (a) C–V curves of capacitors capped with an *ex situ* ALD-HfO_2 layer after exposure to ambient air, the black curve with empty circles indicates the reference sample without ALD-AlO_X layer, the red, orange, and green with 5, 7, and 10 cycles of ALD-AlO_X. (b) The extracted Q_{fix} values range, the right-hand side shows the result for an *ex situ* ALD-HfO_2 capping, the left-hand side shows the results for *in situ* samples without breaking the vacuum between AlO_X and HfO_2 deposition, (c) C–V curves for comparison of the *ex situ* and *in situ* capping, and (d) parallel measured G–V curves.

$-4.5 \times 10^{12}\,cm^{-2}$ or accordingly a relative Q_{fix} induced by the Al-acceptor states of around $-5.5 \times 10^{12}\,cm^{-2}$. The C–V curves (forward sweep) of these four samples comparing the *ex situ* and *in situ* capping deposition are presented in Fig. 8(c).

Clearly, *in situ* capping deposition is highly advantageous for maximizing the negative fixed charge density, which serves as a direct proxy for the hole density induces by modulation doping. The reason for this could be that exposing the ALD-AlO_X monolayer to air (for a limited period of about 1 h) leads to airborne adsorbates, which might deactivate Al-acceptor states. Therefore, the stability of the ALD-AlO_x monolayer upon air exposure is critical for preserving the effectiveness of modulation doping.

The extracted interface trap densities (D_{it}) from the parallel conductance–voltage (G–V) measurement [Fig. 8(d)], obtained using the conductance method,[31] are approximately $4 \times 10^{11}\,cm^{-2}\,eV^{-1}$ for the *ex situ* samples and $\sim 8 \times 10^{11}\,cm^{-2}\,eV^{-1}$ for the *in situ* samples. Within the experimental uncertainties, these D_{it} values are quite similar and, in fact, indicate a slightly lower interface defect density for the *ex situ* sample. Hence, the Si/SiO_2 interface, which is probed by this measurement, is not significantly affected by the *in situ* vs *ex situ* process flows. This suggests that *in situ*/*ex situ* processing predominantly influences the AlO_x/HfO_2 interface, which is not accessed by the G–V measurement.

On the other hand, a significant clockwise hysteresis is reintroduced for the HfO_2 capped SiO_2:Al stack, which points toward an origin based on the band alignment of this stack: Due to the valence and conduction band offsets of HfO_2 compared to ultra-wide bandgap material SiO_2, charges that tunnel

through SiO_2 under accumulation bias conditions are then trapped in HfO_2 behind the SiO_2 band offset. In this case, the hysteresis is just an artifact of the band alignment that only appears in C–V measurements when an electric field is applied over the dielectric.

IV. CONCLUSION

In this work, we have optimized the atomic layer deposition of HfO_2 as a charge-lean capping material to protect the ultra-thin modulation doping (MD) stack, which is highly susceptible to degradation when exposed to ambient air. By using tetrakis(ethylmethylamino)hafnium (TEMAHf), and investigating various deposition conditions, including the choice of oxygen agent (H_2O, O_3, O_2-plasma), deposition temperature, and post-annealing treatment (RTA), we found that H_2O-based TALD at moderate temperatures (200–250 °C) yielded the most promising results. The optimized ALD-HfO_2 films exhibited steep C–V curves, low defect densities, minimal hysteresis, and low fixed oxide charge density ($Q_{fix} < 1 \times 10^{12}\,cm^{-2}$). Moreover, the H_2O-based TALD-HfO_2 films achieved the highest permittivity values ($\varepsilon = 17$) among the investigated capping materials. The long-term stability test confirms that these HfO_2 films maintain reliable performance for at least one year under ambient storage conditions.

Investigation of the thickness and RTA effects on the film characteristics revealed that RTA yielded crystallized monoclinic HfO_2 films with different thicknesses (ca. 5, 15, 30 nm). I–V measurements of the HfO_2 in the MOS-caps type-A configuration showed that thinner films (5 nm) exhibited smaller hysteresis, lower leakage current, and, interestingly, higher breakdown fields, compared to the thicker films (30 nm). However, it should be noted that the thinnest films exhibited the highest density of Q_{fix}.

Integration of the optimized ALD-HfO_2 with the SiO_2:Al MD stack in MOS-caps type-B structures demonstrated its suitability as a capping layer. Notably, *in situ* capping, where the HfO_2 layer is deposited immediately after the AlO_X without breaking vacuum, resulted in 80% higher modulation doping induced fixed charge density of $-4.5 \times 10^{12}\,cm^{-2}$ compared to $-2.5 \times 10^{12}\,cm^{-2}$ for *ex situ* capped samples. This finding emphasizes the critical role of an appropriate capping such as H_2O-grown ALD-HfO_2 to maximize the performance of modulation acceptor doping stacks.

SUPPLEMENTARY MATERIAL

See the supplementary material for more details on the optimization and thickness dependence characteristics of ALD-HfO_2.

ACKNOWLEDGMENTS

The authors acknowledge the German Research Foundation (DFG) for funding via the research grant MADSiNano (No. 456993281). In addition, D.H. acknowledges the funding via a DFG-Heisenberg grant (No. 434030435) and the State Ministry of Science and Cultural Affairs of Saxony (SMWK, Investitionsschwerpunkt, Grant No. 100591077). The authors would like to thank Alexander Schmid (TU Freiberg) for help with the C–V measurements and the valuable discussions that contributed to the analysis of the electrical characterization results.

AUTHOR DECLARATIONS

Conflict of Interest

The authors have no conflicts to disclose.

Author Contributions

Somayeh Shams: Data curation (equal); Formal analysis (equal); Investigation (equal); Methodology (equal); Writing – original draft (equal). **Ingmar Ratschinski:** Investigation (equal); Methodology (supporting); Writing – review & editing (equal). **Daniel Hiller:** Investigation (equal); Supervision (equal); Writing – review & editing (equal).

DATA AVAILABILITY

The data that support the findings of this study are available within the article or its supplementary material and are available from the corresponding author upon reasonable request.

REFERENCES

[1]T. Mikolajick, A. Heinzig, J. Trommer, S. Pregl, M. Grube, G. Cuniberti, and W. M. Weber, Phys. Status Solidi RRL **7**, 793 (2013).
[2]J.-P. Colinge, C.-W. Lee, A. Afzalian, N. D. Akhavan, R. Yan, I. Ferain, P. Razavi, B. O'Neill, A. Blake, M. White, A.-M. Kelleher, B. McCarthy, and R. Murphy, Nat. Nanotechnol. **5**, 225 (2010).
[3]J. Goorissen and A. M. J. G. van Run, Proc. IEE Part B **106**, 858 (1959).
[4]J. C. Ho, R. Yerushalmi, Z. A. Jacobson, Z. Fan, R. L. Alley, and A. Javey, Nat. Mater. **7**, 62 (2008).
[5]J. O'Connell, G. Collins, G. P. McGlacken, R. Duffy, and J. D. Holmes, ACS Appl. Mater. Interfaces **8**, 4101 (2016).
[6]D. J. Norris, A. L. Efros, and S. C. Erwin, Science **319**, 1776 (2008).
[7]G. M. Dalpian and J. R. Chelikowsky, Phys. Rev. Lett. **96**, 226802 (2006).
[8]G. Cantele, E. Degoli, E. Luppi, R. Magri, D. Ninno, G. Iadonisi, and S. Ossicini, Phys. Rev. B **72**, 113303 (2005).
[9]D. König, S. Gutsch, H. Gnaser, M. Wahl, M. Kopnarski, J. Göttlicher, R. Steininger, M. Zacharias, and D. Hiller, Sci. Rep. **5**, 9702 (2015).
[10]D. König, D. Hiller, S. Gutsch, M. Zacharias, and S. Smith, Sci. Rep. **7**, 46703 (2017).
[11]M. Diarra, Y.-M. Niquet, C. Delerue, and G. Allan, Phys. Rev. B **75**, 045301 (2007).
[12]M. V. Fernández-Serra, C. Adessi, and X. Blase, Phys. Rev. Lett. **96**, 166805 (2006).
[13]G. Gupta, B. Rajasekharan, and R. J. E. Hueting, IEEE Trans. Electron Devices **64**, 3044 (2017).
[14]W. Chen, D. Qi, X. Gao, and A. T. S. Wee, Prog. Surf. Sci. **84**, 279 (2009).
[15]H. Méndez, G. Heimel, S. Winkler, J. Frisch, A. Opitz, K. Sauer, B. Wegner, M. Oehzelt, C. Röthel, S. Duhm, D. Többens, N. Koch, and I. Salzmann, Nat. Commun. **6**, 8560 (2015).
[16]D. Hiller, J. Göttlicher, R. Steininger, T. Huthwelker, J. Julin, F. Munnik, M. Wahl, W. Bock, B. Schoenaers, A. Stesmans, and D. König, ACS Appl. Mater. Interfaces **10**, 30495 (2018).
[17]I. Ratschinski, S. Nagarajan, J. Trommer, A. Luferau, M. B. Khan, A. Erbe, Y. M. Georgiev, T. Mikolajick, S. C. Smith, D. König, and D. Hiller, Phys. Status Solidi A **220**, 2300068 (2023).

[18]S. Nagarajan, D. Hiller, I. Ratschinski, D. König, S. C. Smith, T. Mikolajick, and J. Trommer, Adv. Mater. Interfaces **11**, 2300600 (2023).
[19]D. Hiller, D. Tröger, M. Grube, D. König, and T. Mikolajick, J. Phys. D: Appl. Phys. **54**, 275304 (2021).
[20]J. Robertson, Eur. Phys. J. Appl. Phys. **28**, 265 (2004).
[21]M. Shirazi and S. D. Elliott, J. Comput. Chem. **35**, 244 (2014).
[22]K. Kukli, M. Ritala, J. Lu, A. Hårsta, and M. Leskelä, J. Electrochem. Soc. **151**, F189 (2004).
[23]D. K. Simon, P. M. Jordan, T. Mikolajick, and I. Dirnstorfer, ACS Appl. Mater. Interfaces **7**, 28215 (2015).
[24]J. Swerts, N. Peys, L. Nyns, A. Delabie, A. Franquet, J. W. Maes, S. van Elshocht, and S. de Gendt, J. Electrochem. Soc. **157**, G26 (2010).
[25]R. Lo Nigro, E. Schilirò, G. Mannino, S. Di Franco, and F. Roccaforte, J. Cryst. Growth **539**, 125624 (2020).
[26]C. Richter, T. Schenk, U. Schroeder, and T. Mikolajick, J. Vac. Sci. Technol. A **32**, 01A117 (2014).
[27]S. Li, Y. Zhang, D. Yang, W. Yang, X. Chen, H. Zhao, J. Hou, and P. Yang, Phys. B **584**, 412065 (2020).
[28]R. L. Puurunen, A. Delabie, S. van Elshocht, M. Caymax, M. L. Green, B. Brijs, O. Richard, H. Bender, T. Conard, I. Hoflijk, W. Vandervorst, D. Hellin, D. Vanhaeren, C. Zhao, S. de Gendt, and M. Heyns, Appl. Phys. Lett. **86**, 073116 (2005).
[29]K.-M. Kim, J. S. Jang, S.-G. Yoon, J.-Y. Yun, and N.-K. Chung, Materials **13**, 2008 (2020).
[30]K. Shiraishi, K. Yamada, K. Torii, Y. Akasaka, K. Nakajima, M. Konno, T. Chikyow, H. Kitajima, and T. Arikado, Jpn. J. Appl. Phys. **43**, L1413–L1415 (2004).
[31]E. H. Nicollian and A. Goetzberger, Bell Syst. Tech. J. **46**(6), 1055–1133 (1967).